

Article

The Current Spectrum Formation of a Non-Periodic Signal: A Differential Approach

Sergey Sokolov ¹, Daniil Marshakov ²  and Arthur Novikov ^{3,*} 

¹ Computer Technologies and Information Security Faculty, Rostov State University of Economics, 69, Bolshaya Sadovaya, 344002 Rostov-on-Don, Russia; s.v.s.888@yandex.ru

² Computer Systems and Information Security Department, Don State TechFigurnical University, 1, Gagarin square, 344000 Rostov-on-Don, Russia; daniil_marshakov@mail.ru

³ Automotive Faculty, Voronezh State University of Forestry and Technologies named after G.F. Morozov, 8, Timiryazeva, 394087 Voronezh, Russia

* Correspondence: arthur.novikov@vglta.vrn.ru; Tel.: +7-903-650-84-09

Received: 21 December 2019; Accepted: 31 March 2020; Published: 6 April 2020



Abstract: The paper deals with the problem of forming spectra of non-periodic signals in real-time. The disadvantage of the existing approaches is the dependence of the formed spectrum on time as a parameter and the possibility of obtaining the signal spectrum in its original definition only for a fixed time, as well as a high amount of computation. In this regard, a computationally efficient algorithm is proposed for forming a spectrum of non-periodic functions on a time interval that is constantly updated with a given sampling step, which ensures the invariance of the generated spectrum to time as a parameter. The algorithm is based on obtaining differential equations that are based on generalized differentiation with respect to a variable time interval of spectral components and their solving while using the fourth-order Runge–Kutta method. A numerical simulation of the developed algorithm was performed using the MATLAB mathematical modeling package using the example of a substantially non-linear function. Based on the practical results, a comparative evaluation of computational and time complexity has been performed in solving the problem. Based on the obtained experimental results, it is concluded that it is possible to effectively use the proposed algorithm to calculate the current spectrum of non-periodic functions with the requirement of small sampling steps, i.e., when calculating the spectrum in real-time.

Keywords: current time interval; differential equations; generalized differentiation; Runge–Kutta method; spectrum of non-periodic functions; spectrum generation algorithm

1. Introduction

The analysis of the spectra of current physical processes in real time is one of the most important tasks of signal processing [1–3]. This problem is relevant, not only in the analysis of various control and communication systems, but it also finds wide application in navigation systems, seismology, astronomy, and others.

Presently, this problem is solved either by calculating the Fourier transform for function $f(t)$ with a variable upper limit of integration [4–6], or the classical Fourier-series expansion [7–9] on a time interval T_i ($T_i = T_{i+1} + \Delta T$; $i = 1, 2, \dots$) constantly updated with a given sampling interval ΔT :

$$f(t) = \frac{a_0}{2} + \sum_{k=1}^{\infty} a_k \cos k \frac{2\pi}{T_i} t + b_k \sin k \frac{2\pi}{T_i} t, \quad (1)$$

$$a_k = \frac{2}{T_i} \int_0^{T_i} f(t) \cos k \frac{2\pi}{T_i} dt,$$

$$b_k = \frac{2}{T_i} \int_0^{T_i} f(t) \sin k \frac{2\pi}{T_i} dt, k = 0, 1, 2, \dots$$

In the first case, the spectrum that formed depends on time as a parameter, thus obtaining the signal spectrum in its classical definition (that is, independent of time) is possible only at a fixed t . In the second case, there is a large amount of computational costs [9] to reduce which methods of discrete transformation, such as Fast Fourier Transform (FFT) [2,10,11], are widely used. The amount of FFT calculations that require $\sim N \log_2 N$ multiplication operations [10,12] is somewhat reduced as compared to traditional conversion. This does not radically change the situation, since, when calculating the current spectrum, this number of multiplication operations must be performed at each new time step with a constantly increasing time interval. Such shortcomings of both approaches create significant difficulties in their practical use.

2. Theoretical Assumptions

2.1. Task Definition

In this regard, there is a need to develop such an algorithm for calculating the spectrum of non-periodic functions on a time interval that was updated with a given sampling interval, which, on one hand, does not require large computational costs and, on the other hand, provides the formation of the spectrum in its original–classical, definition (1).

2.2. Task Solution

For the construction of this algorithm, the variations Δa_k and Δb_k of spectral coefficients a_k and b_k that are caused by a change in the time interval T_i by the value ΔT are preliminarily found. Using the equation of generalized differentiation by variable T_i (Leibniz formula), we have for the corresponding spectral components:

$$\begin{aligned} \frac{\partial a_k}{\partial T_i} &= -\frac{2}{T_i^2} \int_0^{T_i} f(t) \cos k \frac{2\pi}{T_i} t dt \\ &+ \frac{2}{T_i} \left(\frac{2\pi k}{T_i^2} \int_0^{T_i} f(t) t \sin k \frac{2\pi}{T_i} t dt + f(T_i) \cos k \frac{2\pi}{T_i} T_i \right), \\ \frac{\partial b_k}{\partial T_i} &= -\frac{2}{T_i^2} \int_0^{T_i} f(t) \sin k \frac{2\pi}{T_i} t dt \\ &+ \frac{2}{T_i} \left(-\frac{2\pi k}{T_i^2} \int_0^{T_i} f(t) t \cos k \frac{2\pi}{T_i} t dt + f(T_i) \sin k \frac{2\pi}{T_i} T_i \right). \end{aligned} \tag{2}$$

Considering further that

$$\begin{aligned} \frac{\partial a_k}{\partial k} &= -\frac{2}{T_i} \frac{2\pi}{T_i} \int_0^{T_i} f(t) t \sin k \frac{2\pi}{T_i} t dt, \\ \frac{\partial b_k}{\partial k} &= \frac{2}{T_i} \frac{2\pi}{T_i} \int_0^{T_i} f(t) t \cos k \frac{2\pi}{T_i} t dt, \end{aligned} \tag{3}$$

Equation (2) is written as

$$\begin{aligned} \frac{\partial a_k}{\partial T_i} &= -\frac{1}{T_i} a_k - \frac{k}{T_i} \frac{\partial a_k}{\partial k} + \frac{2}{T_i} f(T_i), \\ \frac{\partial b_k}{\partial T_i} &= -\frac{1}{T_i} b_k - \frac{k}{T_i} \frac{\partial b_k}{\partial k}. \end{aligned} \tag{4}$$

Since k changes discretely in increments of one, an approximation is possible $\frac{\partial a_k}{\partial k} = a_k - a_{k-1}$, $\frac{\partial b_k}{\partial k} = b_k - b_{k-1}$, which allows us to finally write the differential equations that describe the dynamics of changes in spectral coefficients, as follows:

$$\begin{aligned} \frac{\partial a_k}{\partial T_i} &= -\frac{1}{T_i} \cdot [(1+k)a_k - ka_{k-1}] + \frac{2}{T_i} f(T_i), \\ \frac{\partial b_k}{\partial T_i} &= -\frac{1}{T_i} \cdot [(1+k)b_k - kb_{k-1}]. \end{aligned} \tag{5}$$

The search for the solution of differential Equation (5) under known initial conditions leads to the formulation of the Cauchy problem, where the initial conditions are: $T_0 = T_{i-1}$ is the end time of the previous time interval, $a_0 = a_{i-1}$ and $b_0 = b_{i-1}$ are the coefficients that are calculated on the previous interval according to the Equation (1).

In practice, the most common method for solving ordinary differential equations $y = q(x, y)$ is the fourth-order Runge–Kutta method [13–15]. In this case, each step calculates the value of the function $q(x, y)$ of the right side four times; each value $y[i + 1]$ is obtained based on the previous one, according to the equation:

$$y[i + 1] = y[i] + \Delta y[i], \tag{6}$$

where

$$\begin{aligned} \Delta y[i] &= h/6(K_1 + 2K_2 + 2K_3 + K_4); \\ K_1 &= q(x[i], y[i]); \\ K_2 &= q(x[i] + h/2, y[i] + hK_1/2); \\ K_3 &= q(x[i] + h/2, y[i] + hK_2/2); \\ K_4 &= q(x[i] + h, y[i] + hK_3); \end{aligned}$$

h is the size of the grid step according to the argument x .

When calculation spectral coefficients a_k and b_k in Equation (5) in this scheme, the argument $x[i]$ is the variable T_i , the argument $y[i]$ is the coefficients $a_k[i]$, $b_k[i]$. Consequently, the calculation procedure takes the form:

$$\begin{aligned} K_{a1} &= -\frac{(1+k)a_k[i] - ka_{k-1}[i]}{T_i} + \frac{2}{T_i} f(T_i), \\ K_{a2} &= -\frac{(1+k)(a_k[i] + h\frac{K_{1a}}{2}) - k(a_{k-1}[i] + h\frac{K_{1a}}{2})}{T_i + \frac{h}{2}} + \frac{2}{T_i + h/2} f(T_i + h/2), \\ K_{a3} &= -\frac{(1+k)(a_k[i] + h\frac{K_{2a}}{2}) - k(a_{k-1}[i] + h\frac{K_{2a}}{2})}{T_i + h/2} + \frac{2}{T_i + h/2} f(T_i + h/2), \\ K_{a4} &= -\frac{(1+k)(a_k[i] + hK_{3a}) - k(a_{k-1}[i] + hK_{3a})}{T_i + h} + \frac{2}{T_i + h} f(T_i + h), \\ \Delta a_k[i] &= h/6(K_{a1} + 2K_{a2} + 2K_{a3} + K_{a4}), \\ a_k[i + 1] &= a_k[i] + \Delta a_k[i]; \\ K_{b1} &= -\frac{(1+k)b_k[i] - kb_{k-1}[i]}{T_i}, \\ K_{b2} &= -\frac{(1+k)(b_k[i] + h\frac{K_{1b}}{2}) - k(b_{k-1}[i] + h\frac{K_{1b}}{2})}{T_i + h/2}, \end{aligned} \tag{7}$$

$$\begin{aligned}
 K_{b3} &= -\frac{(1+k)(b_k[i] + h\frac{K_{2b}}{2}) - k(b_{k-1}[i] + h\frac{K_{2b}}{2})}{T_i + h/2}, \\
 K_{b4} &= -\frac{(1+k)(b_k[i] + hK_{3b}) - k(b_{k-1}[i] + hK_{3b})}{T_i + h}, \\
 \Delta b_k[i] &= h/6(K_{b1} + 2K_{b2} + 2K_{b3} + K_{b4}), \\
 b_k[i + 1] &= b_k[i] + \Delta b_k[i].
 \end{aligned}$$

The accuracy of the solution of which is largely influenced by the value of the step h of the grid, a numerical estimate of the accuracy of determining the dynamics of changes in the spectral coefficients, given below, was made to analyse the computational efficiency of the obtained equations.

3. Results

3.1. Experimental Design

The numerical simulation of the developed algorithm was carried out using the MATLAB (The MathWorks, Inc., USA) mathematical modeling package, which allows for additionally estimating the time costs for the solution. To assess the accuracy of the proposed algorithms, three essentially nonlinear functions were considered as a test function:

$$\begin{aligned}
 f(t) &= \frac{\sin(t)}{1 + 2\cos^2 2t} \cdot e^{-0.015t}; \\
 f_2(t) &= \sin^2 t + 2e^{0.05t}; \\
 f_3(t) &= (0.5t + \cos(t)) \cdot e^{-0.2t}.
 \end{aligned} \tag{8}$$

The spectra of this function were constructed for time intervals $T_0 = 50.1$ s and $T_0 = 51.0$ s both using classical integral transformations (1) to form the reference spectra and while using the proposed algorithm for the sampling interval $\Delta T = 0.001$ s. The grid step h for the Runge–Kutta algorithm was assumed to be equal $h = 0.0001$.

The evaluation of the comparative results of modeling the values of spectral coefficients $a_k[i]$ and $b_k[i]$ obtained using the integral transformation (1) and the proposed algorithm was carried out according to the following criteria:

- By graphical representation of calculated coefficients and reconstructed signals;
- On the Central Processing Unit (CPU) time during calculations;
- Relative performance, defined as the percentage of the difference between the time estimates of calculations performed using the classical (see Equation 1) and the developed algorithms, and the time of calculation using the classical algorithm; and,
- Based of the standard deviations analysis of the spectral coefficients values $a_k[i]$ and $b_k[i]$ calculated by the above algorithm from the reference values $a_{kr}[i]$ and $b_{kr}[i]$ calculated by the integral transformation (1).

The estimation of the CPU operation time during the calculations was made on the personal computer Intel Core i5-2500 3.30 GHz.

3.2. Numerical Modelling

Figure 1 shows the graphical results of modeling the spectral coefficients $a_{kr}[i]$ and $b_{kr}[i]$ (solid line), $a_k[i]$ and $b_k[i]$ (dotted line) that were obtained using the traditional and the proposed algorithms for the function $f_1(t)$ in the time interval $T_0 = 50.1$ s, respectively.

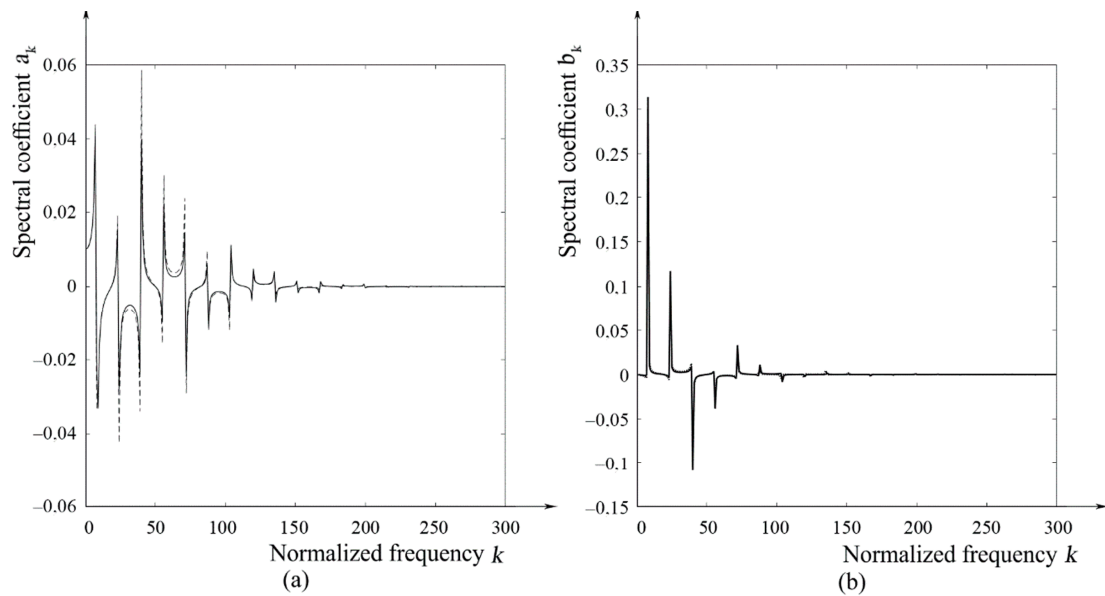


Figure 1. Graphic representation of the spectral coefficients a_k (a) and b_k (b) for the $f_1(t)$ function in time interval $T_0 = 50.1$ s and sampling interval $\Delta T = 0.001$ s.

The CPU operating time in the calculation using the integral transformation (1) was 1.7188 s, in the calculation according to the proposed algorithm -0.0625 s. The relative performance of the proposed algorithm in this case amounted to 96.4%. The mean square deviations of the spectral coefficients were: for the coefficients $a_k[i]$ $s_1 = 0.0020$; and, for the coefficients $b_k[i]$ $s_2 = 0.0018$.

The time signals for the $f_1(t)$ function that was reconstructed from the received spectra are shown in Figure 2. Here, a solid line f_1 shows the restored signal for 50.1 s, as calculated from the spectrum that was obtained using the integral transformation (1), and dotted line from the spectrum obtained using the proposed algorithm.

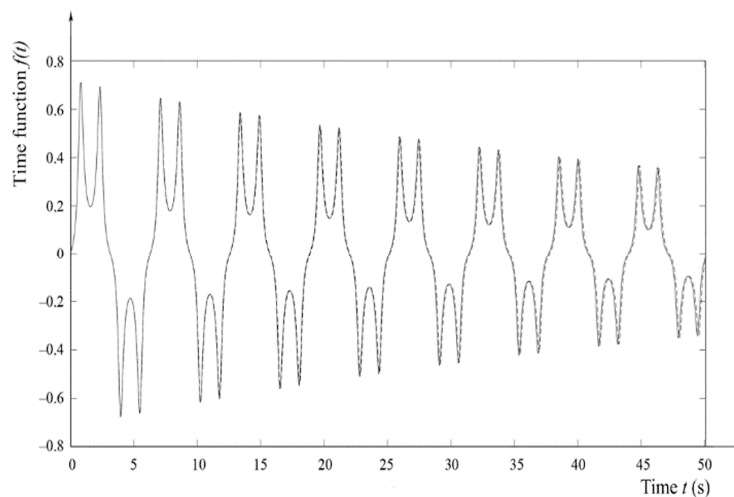


Figure 2. Recovered $f_1(t)$ function signals for the time interval $T_0 = 50.1$ s.

At this time interval (for 10^2 time samples of the current spectrum formation), the coincidence of the spectral coefficients $a_k[i]$ and $b_k[i]$ calculated by the proposed algorithm with the reference values $a_{kr}[i]$ and $b_{kr}[i]$ calculated by the integral transformation (1), as well as the restored signals, is almost complete, as can be seen from the simulation results. At the same time, the time spent on the process of calculating the current spectrum in the proposed algorithm decreased by more than 96% when compared to the classical one.

Figure 3 shows the graphical results of modeling the spectral coefficients $a_{kr}[i]$ and $b_{kr}[i]$ (solid line), $a_k[i]$ and $b_k[i]$ (dotted line) that were obtained using the traditional and the proposed algorithms for the function $f_1(t)$ in the time interval $T_0 = 51.0$ s, respectively.

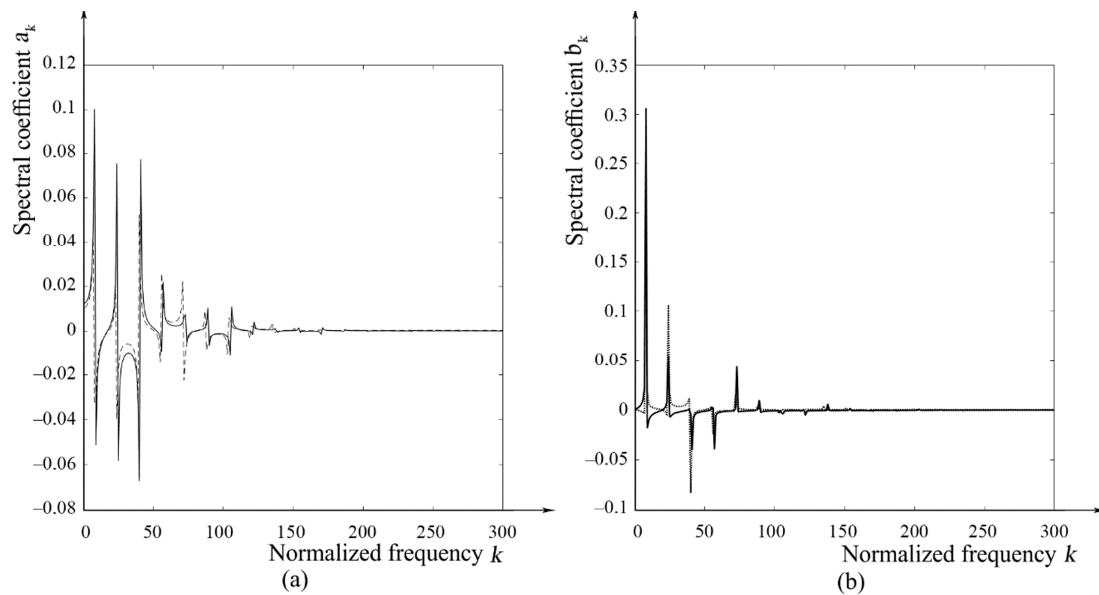


Figure 3. Graphic representation of the spectral coefficients a_k (a) and b_k (b) for the $f_1(t)$ function in time interval $T_0 = 51.0$ s and sampling interval $\Delta T = 0.001$ s.

The CPU operating time in the calculation using the integral transformation (1) was 1.8750 s, in the calculation according to the proposed algorithm -0.3594 s. The relative performance of the proposed algorithm in this case amounted to 80.8%. The mean square deviations of the spectral coefficients were: for the coefficients $a_k[i]$ $s_1 = 0.0147$; and, for the coefficients $b_k[i]$ $s_2 = 0.0089$.

The time signals for the $f_1(t)$ function reconstructed from the obtained spectra are shown in Figure 4. Here, a solid line shows the recovered signal for 51.0 s, calculated from the spectrum obtained using the integral transformation (1), and dotted line from the spectrum that was obtained using the proposed algorithm.

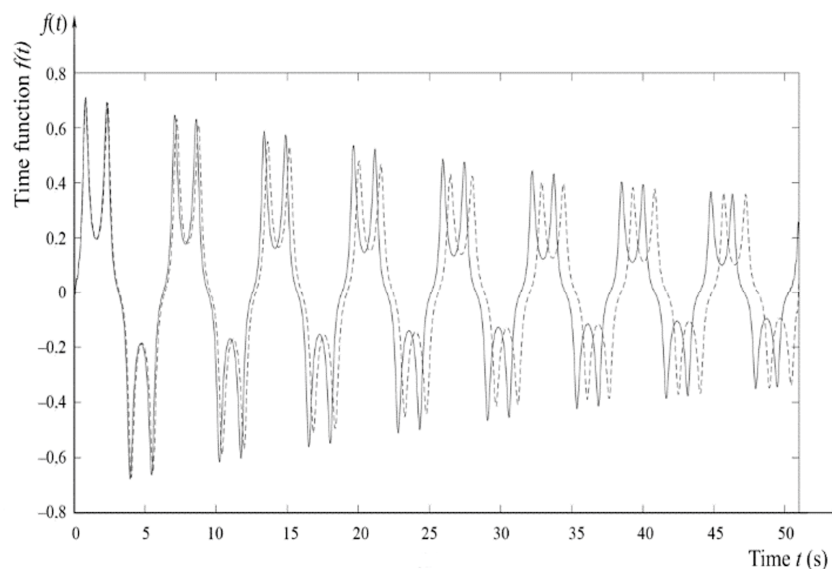


Figure 4. Recovered $f_1(t)$ function signals for the time interval $T_0 = 51.0$ s.

At this time interval $T_0 = 51.0$ s (for 10^3 time samples of the current spectrum formation), the coincidence of the spectral coefficients that were calculated by the given algorithm with the reference ones, as well as the reconstructed signals, has somewhat deteriorated when compared to the previous time interval, which is due to the accumulation of step-by-step calculation errors in the proposed recurrent algorithm. However, nevertheless, the time spent on the process of calculating the current spectrum in the proposed algorithm was still more than 80% less as compared to the classical one.

Since the proposed algorithm shows fairly stable results for small time intervals, the results of numerical simulation for the $f_2(t)$ and $f_3(t)$ functions are immediately presented for the time interval $T_0 = 51.0$ s, after which a generalized evaluation of the results for all three functions for the time intervals $T_0 = 50.1$ s and $T_0 = 51.0$ s.

Figure 5 shows the graphical results of modeling the spectral coefficients $a_{kr}[i]$ and $b_{kr}[i]$ (solid line), $a_k[i]$ and $b_k[i]$ (dotted line) that were obtained using the traditional and the proposed algorithms for the function $f_2(t)$ in the time interval $T_0 = 51.0$ s, respectively.

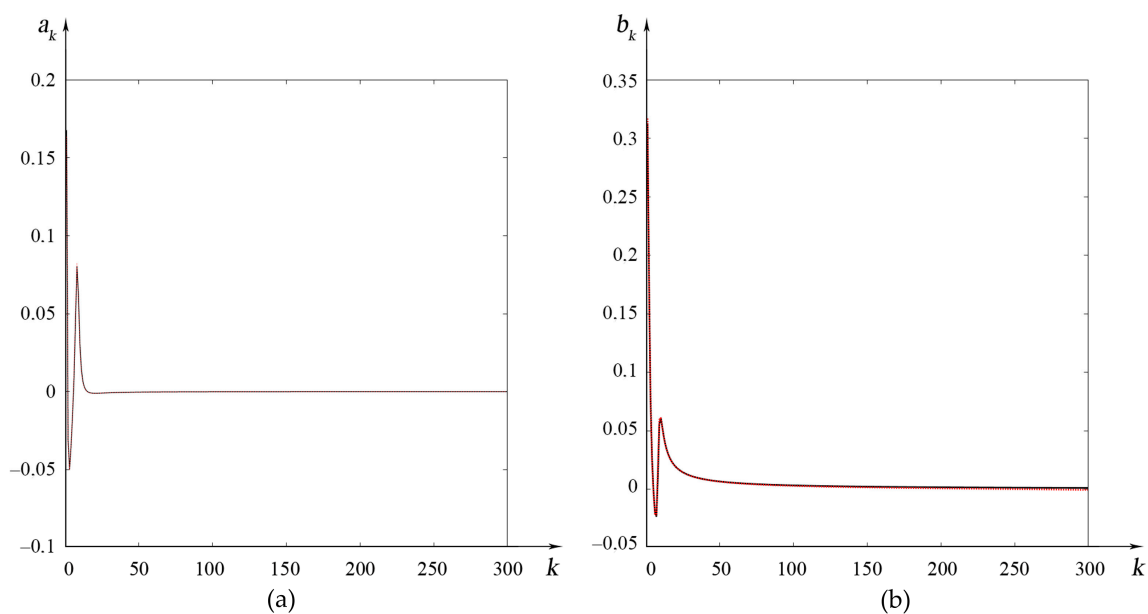


Figure 5. Graphic representation of the spectral coefficients a_k (a) and b_k (b) for the $f_1(t)$ function in time interval $T_0 = 51.0$ s and sampling interval $\Delta T = 0.001$ s.

The CPU operating time in the calculation using the integral transformation (1) was 1.5938 s, in the calculation according to the proposed algorithm –0.3281 s. The relative performance of the proposed algorithm in this case amounted to 79.4%. The mean square deviations of the spectral coefficients were: for the coefficients $a_k[i]$ $s_1 = 0.0006512$; and, for the coefficients $b_k[i]$ $s_2 = 0.00082342$.

Figure 6 shows the time signals for the $f_2(t)$ function that was reconstructed from the obtained spectra. Here, a solid line shows the recovered signal for 51.0 s, which was calculated from the spectrum obtained using the integral transformation (1), and the dotted line from the spectrum that was obtained using the proposed algorithm.

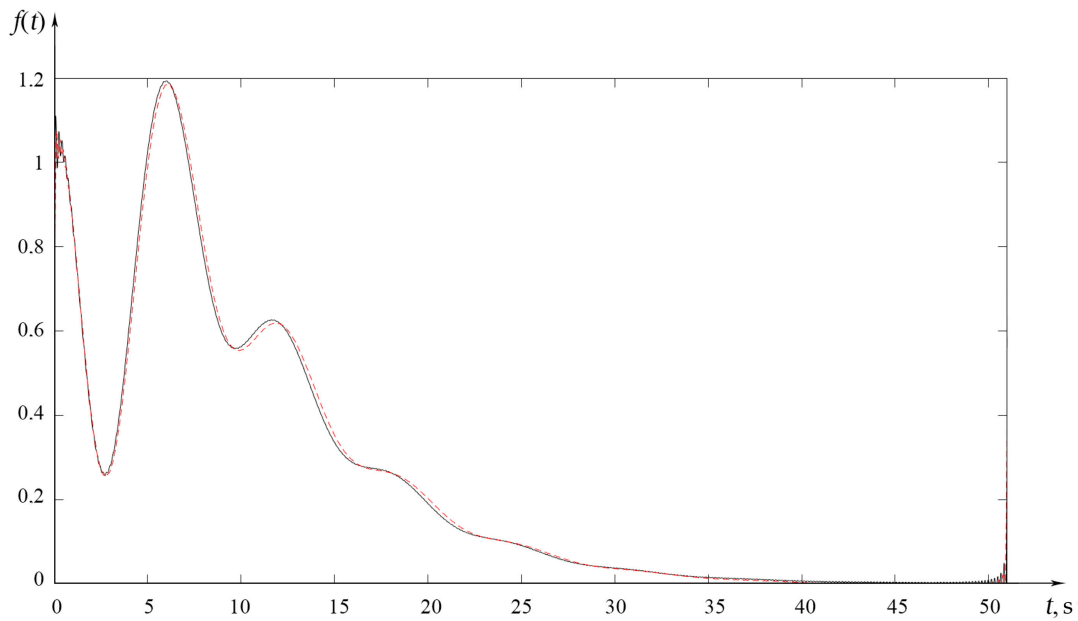


Figure 6. Recovered $f_2(t)$ function signals for the time interval $T_0 = 51.0$ s.

Figure 7 shows the graphical results of modeling the spectral coefficients $a_{kr}[i]$ and $b_{kr}[i]$ (solid line), $a_k[i]$ and $b_k[i]$ (dotted line) obtained while using the traditional and the proposed algorithms for the function $f_3(t)$ in the time interval $T_0 = 51.0$ s, respectively.

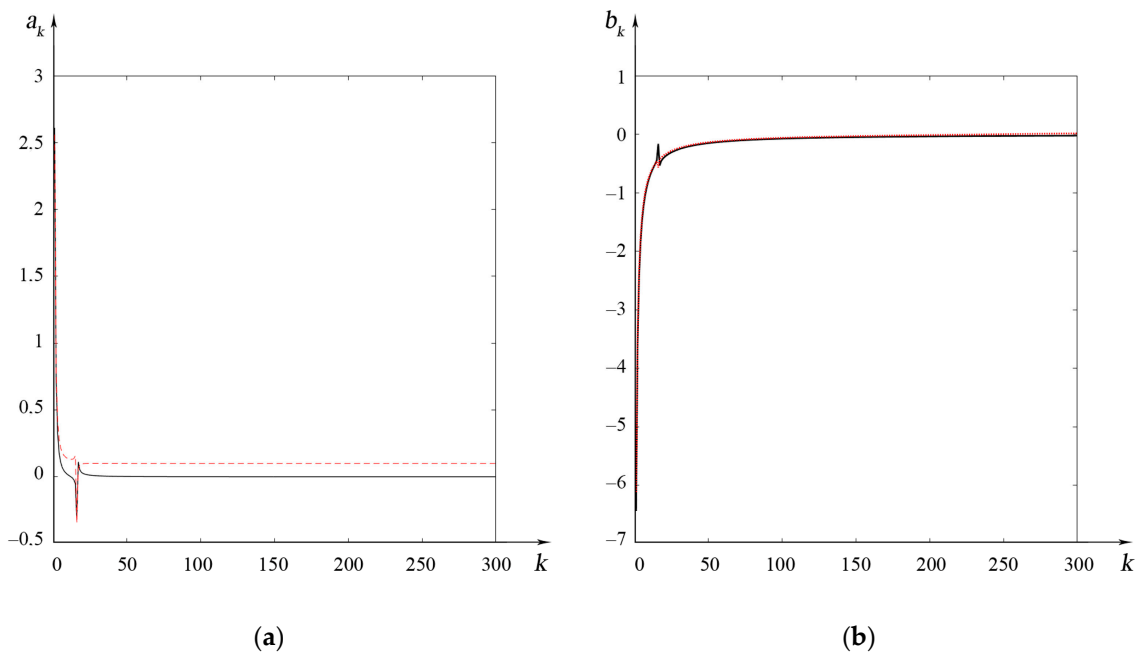


Figure 7. Graphic representation of the spectral coefficients a_k (a) and b_k (b) for the $f_2(t)$ function in time interval $T_0 = 51.0$ s and sampling interval $\Delta T = 0.001$ s.

The CPU operating time in the calculation using the integral transformation (1) was 1.6250 s, in the calculation according to the proposed algorithm 0.3281 s. The relative performance of the proposed algorithm in this case amounted to 79.8%. The mean square deviations of the spectral coefficients were: for the coefficients $a_k[i]$ $s_1 = 0.0172$; and, for the coefficients $b_k[i]$ $s_2 = 0.0342$.

Figure 8 shows the time signals for the $f_3(t)$ function that was reconstructed from the obtained spectra. Here, a solid line shows the recovered signal for 51.0 s, as calculated from the spectrum that

was obtained using the integral transformation (1), and dotted line from the spectrum obtained using the proposed algorithm.

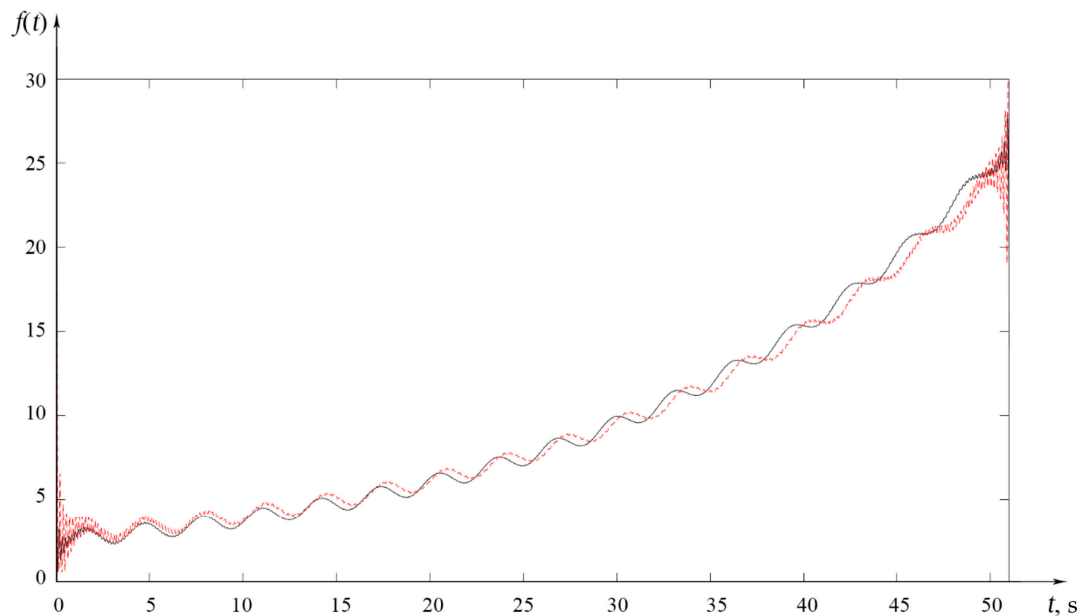


Figure 8. Recovered $f_3(t)$ function signals for the time interval $T_0 = 51.0$ s.

3.3. Evaluation of Numerical Modelling

Table 1 provides a generalized estimate of the results of numerical simulation for functions $f_1(t)$, $f_2(t)$, and $f_3(t)$ at time intervals $T_0 = 50.1$ s and $T_0 = 51.0$ s.

Table 1. Generalized evaluation of the results of numerical modeling.

Time Interval	$T_0 = 50.1$ s			$T_0 = 51.0$ s		
	Standard Deviation for $a_k[i]$	Standard Deviation for $b_k[i]$	Performance, %	Standard Deviation for $a_k[i]$	Standard Deviation for $b_k[i]$	Performance, %
$f_1(t)$	0.0020	0.0018	96.4	0.0147	0.0089	80.8
$f_2(t)$	0.000066253	0.0004806	97.0	0.0006512	0.00082342	79.4
$f_3(t)$	0.0020	0.0107	98.8	0.0172	0.0342	79.8

As follows from the results, for all three functions, the performance estimates have approximately the same values—the relative performance of the process of calculating the current spectrum for the time interval $T_0 = 50.1$ s is more than 96%, for $T_0 = 51.0$ s about 80%.

In order to assess the effect of the value of the time interval on the growth of errors that were caused by the accumulation of incremental error calculation in the proposed algorithm, for the considered nonlinear functions are constructed based on changes (Figure 9) in the values of standard deviation values of the spectral coefficients $a_k[i]$ (dashed line) and $b_k[i]$ (solid line) recovered signals in the interval from 50.1 to 60.0 s.

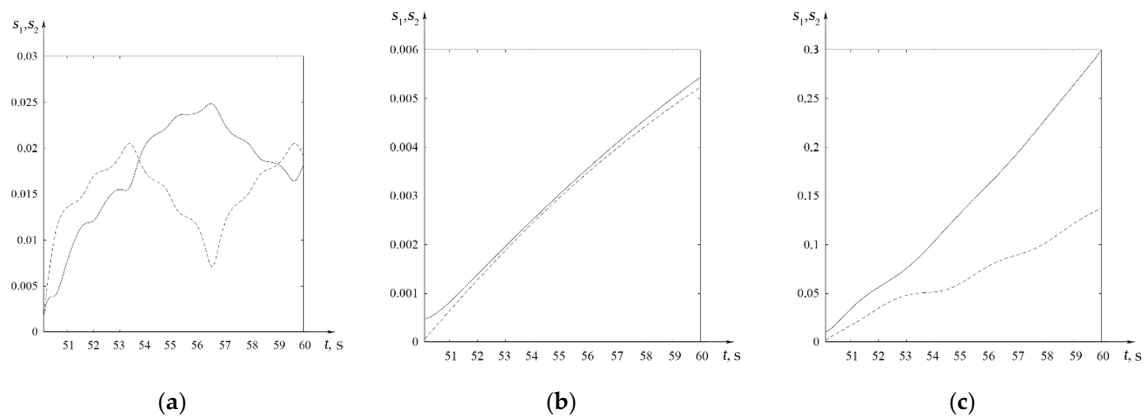


Figure 9. Dependences of changes in the mean square deviations of spectral coefficients $a_k[i]$ and $b_k[i]$ for $f_1(t)$ (a), $f_2(t)$ (b), and $f_3(t)$ (c) functions in the range from 50.1 s to 60 s.

From the analysis of these dependencies, we can conclude that the temporal nature of the mismatch of spectral coefficients depends on the type of function being modeled and the nature of its nonlinearity. Accordingly, for the function $f_1(t)$ deviation of the recovered spectrum above the value of 0.005 is observed at 52 s, for the function $f_2(t)$ at 59 s, for the function $f_3(t)$ at 51 s. In this case, for 51 s (Figure 8), the recovered signal generally shows a slight deviation, but fluctuations that occur at the spectrum boundaries lead to an increase in the standard deviations of the spectral coefficients.

4. Conclusions

The results of numerical modeling allow for drawing a conclusion regarding the possibility of effective practical use of the proposed approach to the calculation of the current spectrum of non-periodic functions under the requirement of small sampling steps (i.e., when calculating the spectrum in real time). In comparison with the most effective method of spectral characteristics formation—FFT, the developed algorithms have the following advantages. Firstly, their number of multiplication and addition operations at each step is constant and it does not depend on the increasing number N of time samples of the signal, being determined by the step of its sampling and the current value T of the increasing time interval and, secondly, this number of operations is incommensurably small when compared to the constantly increasing number of FFT operations $N \log_2 N$ at the current interval.

The implementation of the developed algorithm is particularly relevant in systems of measurement and the spectral processing of broadband signals in real time—telecommunications, navigation, and others.

Author Contributions: Conceptualization, S.S.; methodology, S.S. and D.M.; formal analysis, S.S. and A.N.; investigation, S.S., A.N.; writing—original draft preparation S.S., D.M. and A.N.; writing—review and editing S.S., D.M. and A.N.; supervision, S.S. All authors have read and agreed to the published version of the manuscript.

Funding: This research was funded by RFBR, grant number 18-07-00126.

Conflicts of Interest: The authors declare no conflict of interest.

References

1. Dyakonov, V. Modern digital spectrum analyzers. *Components Technol.* **2010**, *5*, 185–195.
2. Isermann, R.; Münchhof, M. *Identification of Dynamic Systems: An Introduction with Applications*; Springer: Berlin/Heidelberg, Germany, 2011; ISBN 978-3-540-78878-2.
3. Iglesias, V.; Grajal, J.; Sanchez, M.A.; Lopez-Vallejo, M. Implementation of a Real-Time Spectrum Analyzer on FPGA Platforms. *IEEE Trans. Instrum. Meas.* **2015**, *64*, 338–355. [[CrossRef](#)]
4. Sergienko, A.B. *Digital Signal Processing*, 3rd ed.; BHV-Petersburg: St. Petersburg, Russia, 2011; ISBN 5977506066.

5. Oppenheim, A.V.; Schafer, R.W. *Discrete-Time Signal Processing*, 3rd ed.; Pearson: London, UK, 2010.
6. Lyons, R.G. *Understanding Digital Signal Processing*, 3rd ed.; Prentice Hall PTR: Upper Saddle River, NJ, USA, 2004; ISBN 8131764362.
7. Marks, R.J., II. *The Joy of Fourier: Analysis, Sampling Theory, Systems, Multidimensions, Sto-Chastic Processes, Random Variables, Signal Recovery, POCS, Time Scales, & Applications*; Baylor University: Waco, TX, USA, 2006.
8. Blahut, R.E. *Fast Algorithms for Signal Processing*; Cambridge University Press: New York, NY, USA, 2010; ISBN 1139487957.
9. Bracewell, R.N. *The Fourier Transform and Applications*; McGraw Hill: Singapore, 2000.
10. Averbchenko, A.P.; Zhenatov, B.D. Estimation of the gain of computational costs of Hartley transform before Fourier transform. *Omsk Sci. Bull.* **2015**, *2*, 190–194.
11. Avramchuk, V.S.; Yakovleva, E.M. Application of lattice periodic functions in spectral analysis of narrowband periodic signals. *Bull. Tomsk Politech. Univ.* **2006**, *309*, 40–44.
12. Bogner, R.E.; Constantinides, A.G. *Introduction to Digital Filtering*; Wiley: New York, NY, USA, 1975; ISBN 0471085901.
13. Chakraverty, S.; Mahato, N.R.; Karunakar, P.; Rao, T.D. *Advanced Numerical and Semi-Analytical Methods for Differential Equations*; Wiley: Hoboken, NJ, USA, 2019; ISBN 9781119423423.
14. Korolova, O.; Popp, M.; Mathis, W.; Ponick, B. Performance of Runge-Kutta family numerical solvers for calculation of transient processes in AC machines. In Proceedings of the 2017 20th International Conference on Electrical Machines and Systems (ICEMS), Sydney, NSW, Australia, 11–14 August 2017; pp. 1–6.
15. Radzi, H.M.; Majid, Z.A.; Ismail, F.; Suleiman, M. Four step implicit block method of Runge-Kutta type for solving first order ordinary differential equations. In Proceedings of the 2011 Fourth International Conference on Modeling, Simulation and Applied Optimization, Kuala Lumpur, Malaysia, 19–21 April 2011; pp. 1–5.



© 2020 by the authors. Licensee MDPI, Basel, Switzerland. This article is an open access article distributed under the terms and conditions of the Creative Commons Attribution (CC BY) license (<http://creativecommons.org/licenses/by/4.0/>).